Homogeneous fluorescence readouts for miniaturized high-throughput screening: theory and practice

Andrew J. Pope, Ulrich M. Haupts and Keith J. Moore

It is widely recognized that fluorescence techniques represent the most important future detection method for miniaturized ultra-high-throughput screening. However, such techniques encompass many different approaches, each with its own particular set of advantages and
limitations. Here, the authors summarize each of the major fluorescence techniques and explain the underlying principles that form the basis for a theory-led strategy to readout selection and assay design.

The notion that fluorescence techniques will form the core detection technology underlying miniaturized ultra-high-throughput screening (uHTS) systems in the future arises largely from the sensitivity of fluorescence measurements, which now extend routinely to the single molecule level (see section on fluorescence correlation spectroscopy). However, an equally important facet of the use of these techniques is the ability to use different aspects of fluorescence output (for example, lifetime, brightness, anisotropy and energy transfer) to construct assays that do not require separation steps and that have an intrinsically higher information content, which can be used for internal validations and interference correction, for example. Moreover, given some simplifying assumptions, relatively straightforward formalisms can be used to describe each of these processes and allow prediction of experimental results and definition of the desired direction for future developments. This review outlines some of these formalisms as they apply to approaches commonly employed in uHTS, and relates the predictions from them with real-life observations of miniaturized homogeneous fluorescence-based assays. Table 1 summarizes the major advantages and disadvantages (or limitations) of each technique.

Fluorescence basics

For the following discussion it is necessary to introduce some basic quantitative descriptors of fluorescence and to make a few introductory comments about the various techniques and relevant instrumentation that will be subsequently discussed.

Macroscopic fluorescence intensity (I_F) is linearly related to fluorophore concentration up to an absorption of ~0.02–0.05.

$$I_F = \Phi_F I_0 (1 - 10^{-\epsilon c l}) \quad (1)$$

where I_0 is the intensity of the light source, ϵ is the molar absorptivity, l is the pathlength and c is the fluorophore concentration

Andrew J. Pope* and **Ulrich M. Haupts**, Molecular Interactions and New Assay Technologies, SmithKline Beecham Pharmaceuticals, New Frontiers Science Park, Third Avenue, Harlow, UK CM19 5AW. **Keith J. Moore**, Lead Discovery Unit, GlaxoWellcome, Research and Development, Gunnels Wood Road, Stevenage, Hertfordshire, UK SG1 2NY. *tel: +44 1279 627583, fax: +44 1279 627699, e-mail: Andrew_J_Pope@sbphrd.com

 1359-6446/99/$ – see front matter PII: S1359-6446(99)01340-9

Fluorescence quantum yield (Φ_F) *and observed lifetime* (τ_F) are determined by the summed rate constants for radiative (Γ) and nonradiative (k_n) processes.

$$\Phi_F = \Gamma/(\Gamma + k_n) \quad (2)$$

i.e. quanta emitted/quanta absorbed

$$\tau_F = \Phi_F \tau_n \quad (3)$$

The observed fluorescence lifetime is related to the average time spent in the excited state. In prompt fluorescence, emission arises directly from singlet state excitation and typically has a short lifetime (e.g. fluorescein and rhodamine: τ_F ~4 ns). Some fluorophores (e.g. Ln^{3+} ions as chelates or cryptate complexes) exhibit long lifetimes (τ_F ~1 ms) owing to luminescence emission from the triplet state with rate constant, K_t (Fig. 1).

Processes affecting nonradiative paths to ground state (energy transfer and environment) affect quantum yield and lifetime. For any given interaction, these effects should be specific and can be used for quality control purposes (e.g. interference correction).

Fluorescence measurements

Fluorescence measurements are made in several ways (Table 1) each with their own specific advantages and limitations. Macroscopic (average ensemble) techniques involve the measurement of integrated signals from a particular optical collection volume (normally a significant proportion of the assay well). Macroscopic fluorescence assay techniques that have uHTS applications include:

Prompt fluorescence intensity (FLINT). The change in steady-state total light output is monitored, for example, using fluorescent enzyme substrates or in resonance energy transfer systems (see below). With the exception of systems such as these, the design of FLINT assays is poorly predictive and, as total fluorescence is measured, test compound inner-filter and autofluorescence effects can be difficult to detect and correct for.

Fluorescence anisotropy/polarization (FA/FP). The excitation light is typically polarized and emission is measured in parallel and perpendicular orientations (see below). Particularly for binding reactions, the relationship between fluorescence anisotropy and molecular properties can be predicted (see below), allowing intelligent assay design. In addition, as anisotropy is a ratiometric technique, it is inherently less prone to interference from inner-filter effects and contains internal quality control information (e.g. total intensity versus anisotropy).

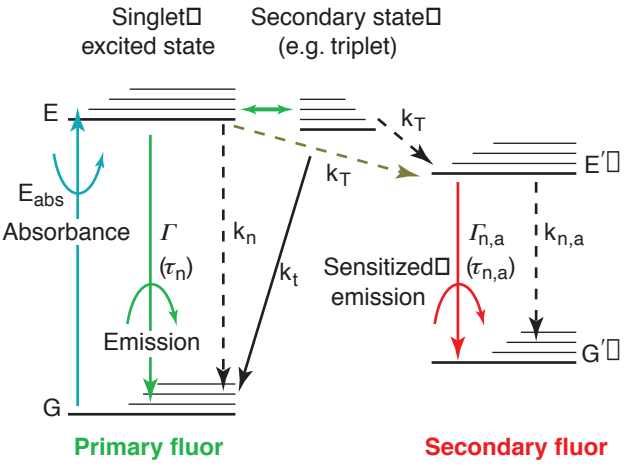

Figure 1. *Simplified Jablonski diagram showing the basic principles of fluorescence. For each electronic energy state (G, G′, E and E′) several vibrational energy levels are present indicated by the closely packed horizontal lines – the higher energy states being at the top of the figure. The resting energetic state of a fluorophore is in the lowest vibrational level of the low energy, ground state (G or S_0 state), from which absorption of a photon with E_{abs} leads to excitation of the fluorophore (typically within 10^{-15} s) and subsequent relaxation (typically in 10^{-12} s) into the lowest vibrational level of the excited singlet state (E or S_1). For simple fluorophores, the energy is dissipated either via radiative processes (with a rate constant Γ) and hence fluorescence emission or via non-radiative processes such as thermal dissipation (with rate constant k_n) which does not yield a fluorescence output. The energy can also be transferred non-radiatively from the excited state of a donor (E) to the excited state of an acceptor (E′) either directly or via an intermediate electronic state (e.g. the triplet state). Direct transfer occurs on a nanosecond timescale (prompt energy transfer), whereas transfer via the triplet state occurs in the micro- to millisecond timescale – this is the basis of time-resolved fluorescence assays. The energy from the excited state of the acceptor can similarly be dissipated via radiative ($\Gamma_{n,a}$) and non-radiative ($k_{n,a}$) pathways to the ground state (G′) with the former yielding a fluorescence emission characteristic of the acceptor.*

Table 1. Advantages and disadvantages/limitations of fluorescence techniques for the establishment of miniaturized homogeneous screening assays

Technique	Advantages	Disadvantages/limitations
Prompt intensity (FLINT)	Simple Suitable for fluorigenic assays Readily miniaturized	Little information for quality control Can suffer from inner-filter and autofluorescence interference
Anisotropy (FA)	Simple, reasonably predictive Insensitive to inner-filter effects Ratiometric technique Improved well-level quality control Suitable for small (<15 kDa) ligands	Local motion (propeller) effects Can suffer from autofluorescence Suitability limited by lifetime of dye, ligand size and molecular weight change Dynamic range limited
Prompt energy transfer (FRET)	Simple, reasonably predictable Suitable for short inter/intramolecular distances (<5 nm) Range of available donors and acceptors	Can suffer from inner-filter and autofluorescence interference Limited to short distances to obtain high signal changes Most dyes monitor only donor quenching
Time-resolved energy transfer (TRET)	Reasonably predictable and robust Suitable for long distances (5–10 nm) Reduced autofluorescence interference Sensitive/miniaturizable	Labelling with donor/acceptor often more complex/problematic (e.g. steric hindrances) Limited choice of donor/acceptors Nonspecific energy transfer limits background
Fluorescence correlation spectroscopy (mass-dependent FCS)	Completely insensitive to miniaturization in the pl–μl range Predictable with wide dynamic range (<1 kDa to >10 mDa) No local motion (propeller) effects Primarily independent of dye lifetime or wavelength Large number of parameters obtained for well-level quality control	Needs large mass difference (>10-fold) Read times can be slow (2 s) at subnanomolar concentrations of ligands Requires complex instrumentation/data processing
Fluorescence correlation spectroscopy (mass-independent FCS)	Insensitive to miniaturization Removes requirement for mass-dependence during interaction Confocal FCS equivalent of FLINT/FRET/FA with improved well-level quality control and reduced/no distance dependence of the signal No change in overall intensity required for assay configuration Cross-correlation predictable and generically applicable	Currently emerging range of techniques with limited application thus far Although simple mass-independent FCS and cross-correlation FCS are rapid, more complex signal-processing techniques currently have low throughput Requires complex instrumentation/data processing Requires improved labelling chemistry

Time-resolved fluorescence (TRF). Long-lived emissions (e.g. from Ln^{3+}) are monitored normally at a fixed time (e.g. 200 μs) after flash illumination, when prompt fluorescence and other background signals (e.g. source light scattering) have decayed. This yields very high levels of sensitivity. More recently, homogeneous assay systems based on time-resolved energy transfer (TRET) have been implemented for HTS usage[1–3].

Fluorescence lifetime measurements. Fluorophore lifetimes are measured directly using either pulsed or phase-modulation techniques[4,5]. Although the direct measurement of lifetimes is not yet available in HTS (i.e. microplate) compatible instrumentation, this approach has considerable promise in providing additional quality control via discrimination of the 'real' lifetime signal (lifetime discriminated intensity, LDI) associated with the biological interaction from spurious background signals (e.g. from light scattering or test compound autofluorescence).

By contrast to these macroscopic fluorescence assays, fluorescence correlation spectroscopy (FCS) involves monitoring quantal bursts from individual fluorophore molecules within a tightly focused confocal element (volume ~1 fl). This introduces some unique advantages, not least because the observation volume is always much less than the assay volume[6–8]. This technique is discussed in more detail in the section on FCS.

Further considerations

Fluorescence intensity (I_F) is affected by light absorption effects either from the fluorophore itself or from test compounds. The latter problem can be addressed in several ways:

- In prompt fluorescence assays, dyes with relatively long wavelengths are used, well away from interfering chromophores and fluorophores in test compound sets.
- In TRF using Ln^{3+} chelates or cryptates that are excited at near-UV wavelengths (e.g. 340 nm), correction schemes are always adopted to correct for excitation light absorption.
- In FCS, the proximity of the small focused observation volume to the plate surface minimizes the pathlength for absorption effects. In addition, FCS is intrinsically insensitive to dim fluorophores (see section on FCS).

In the absence of test compounds, FLINT/FP assays can be performed on current HTS-compatible instrumentation with reasonable precision at fluorophore concentrations of ~0.5–10 nM, depending upon the instrument and dye used. However, the observed signal from a typical HTS well is a function of contributions from the fluorophore and from all other signals (i.e. background). Common sources of background fluorescence include autofluorescence from the plates (for nonconfocal techniques), from the cells or cell membranes and from light scattering, either resulting from partial insolubility of test compounds or from reflections within the optic path. However, the predominant source of background signal during HTS appears to be the autofluorescence of test compounds such that significant distortions in the signal (in the presence of compounds) can occur under conditions where the measurement in the absence of compounds is robust. Consequently, typical fluorophore concentrations of ⩾10 nM are required for robust HTS based on prompt fluorescence intensity using current microtitre plate (MTP) readers. In TRF, autofluorescence from the file compounds and the MTP is minimal, so that most background signal arises from nonspecific (diffusion limited) energy transfer and from the detection of donor emission (e.g. from Eu^{3+}) in the acceptor (e.g. allophycocyanin, APC) channel.

Predicting macromolecular properties

Attempts to predict molecular properties to assess the utility of different fluorescence assay strategies at the design stage always involve several simplifying assumptions. Nonetheless, useful information can be derived from calculations based on, for example, only the molecular weight of the assay components. This approach is clearly not capable of yielding very precise estimates but can often give a useful guide to which approaches are (or are not) most likely to work. This strategy is extremely useful in minimizing assay design cycle times and eliminating approaches that are unlikely to be fruitful for a given target. Some of the relevant formalisms follow.

By assuming that proteins have a simple spherical shape, the hydrodynamic molecular radius (r) can be estimated easily from the mass (M) (Fig. 2a).

$$r = \left[\frac{3M}{4\pi N_a}(v + \delta)\right]^{1/3} \quad (4)$$

where M is the molecular mass (Da), N_a is Avagadro's number (6.022×10^{23} mol^{-1}), v is the specific volume (cm^3 g^{-1}) and δ is the specific hydration volume (cm^3 g^{-1}).

This in turn allows the diffusion coefficient (D) and molecular rotation rates [described by the rotational correlation time (τ_c) and rotational relaxation time (ρ)] to be calculated directly.

$$D = kT/6\pi nr \quad (5)$$

$$\tau_c = \rho/3 \quad (6)$$

$$\rho = 3M(v + \delta)n/RT \quad (7)$$

where n is the visocity (g cm^{-1} s^{-1}), k is the Boltzmann constant (1.381×10^{-23} J K^{-1}), T is the absolute temperature (e.g. 293 K) and R is the gas constant (8.314 J mol^{-1} K^{-1}).

Molecular rotation rates are directly related to mass (typical value for a protein: ρ ~0.68 ns kDa^{-1}). By contrast, D is related to the reciprocal of r (Eqn 5), which in turn is a function of the cubed root of mass. Figure 2b shows predictions of the effect of globular protein mass on D, r, ρ and τ_c.

In energy transfer measurements of binding reactions, a very approximate estimate of the maximum donor–acceptor distance possible (which places limits on the energy transfer pair; see following section) can be obtained from the mean hydrodynamic radius (r). In Figure 2a an example is given for a dimerization reaction using the maximum donor–acceptor distance, $4r$.

For elongated molecules such as peptides or nucleic acids, the end-to-end distance in an extended conformation can

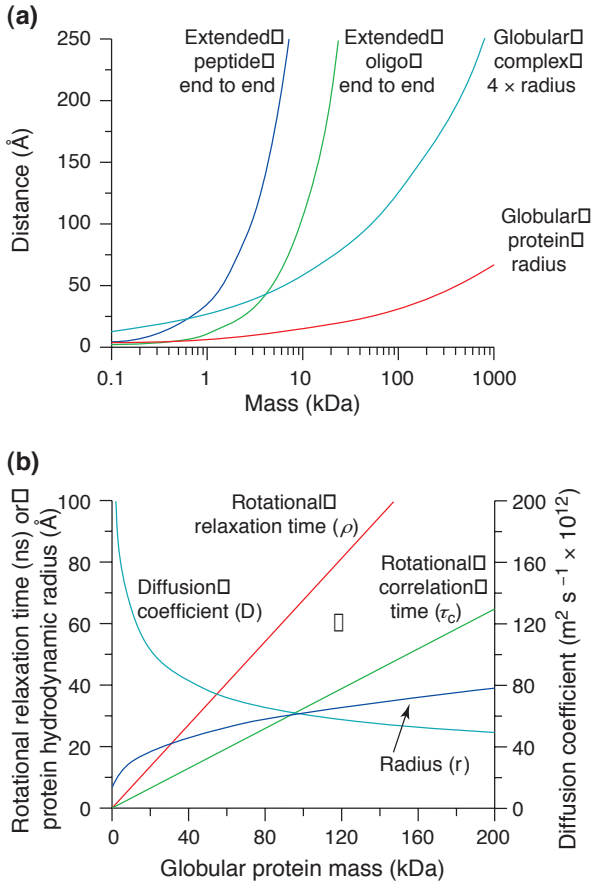

Figure 2. *Predicted properties of macromolecules as a function of mass. (a) Radius (*r*) of globular proteins predicted from Eqn 4 and end-to-end distance of extended oligonucleotides or peptides, respectively. (b) Radius (*r*), diffusion coefficient (*D*), rotational relaxation time (*ρ*) and rotational correlation time (τ_c) calculated for spherical globular proteins as described in the text.*

be estimated from the known bond lengths (i.e. peptide ~3.82 Å per amino acid, oligonucleotide ~3.4 Å per base; Fig. 2a). For elongated macromolecules such as these, estimates of *D* (Eqn 8) and molecular rotation rates can be adjusted to take shape into account[9].

$$D = AkT/6\pi nr \tag{8}$$

where *A* is an asymmetry correction factor:

$$A = \frac{\ln(L/d) + 0.877}{(L/d) - [0.1/(L/d)^2]} \tag{9}$$

and *L*/*d* is the ratio of length to diameter.

Fluorescence resonance energy transfer

Nonradiative transfer of excitation energy between a fluorescent donor and a suitable energy acceptor has long been recognized as a useful means to detect molecular proximities[10,11]. Förster theory[12] provides a reasonable description of this process and can provide useful insights into the design of systems and directions for future improvements. Some of the relevant formalisms follow.

The distance for half-transfer efficiency (R_0, in Å) depends upon the spectral overlap between donor and acceptor (*J*, in M^{-1} cm^{-3}), donor quantum yield (Φ_d), donor–acceptor dipole-orientation factor (κ^2) and refractive index of the medium (*n*), but can be calculated for any pair (Fig. 3a).

$$R_0 = 9.8 \times 10^3 (J\kappa^2 \Phi_d n^{-4})^{1/6} \tag{10}$$

$$J = \int_0^\infty \epsilon_A(\lambda) \cdot I_d(\lambda) \cdot \lambda^4 \cdot d\lambda \tag{11}$$

where ϵ_A is the extinction coefficient of the acceptor, I_d is the intensity of the donor and λ is the wavelength.

Rate of energy transfer (k_T) (in s^{-1}). In any energy transfer system, the major unknown is κ^2 (Eqn 12), which can have the range 0–4, but is normally assumed to be two-thirds (i.e. 0.667). Figure 3b shows the effect of variations in Φ_d, *n* and κ^2, within normal ranges, on R_0, and hence, on K_T (Eqn 13).

$$\textit{rate of energy transfer}\,(k_T) = 8.71 \times 10^{23} (r^{-6} k^2 J n^{-4} \phi_d k_F)\ s^{-1} \tag{12}$$

or:

$$k_T = (1/\tau_d)(R_0/r)^6 \tag{13}$$

where *r* is the donor–acceptor distance (Å), k_F is the rate constant for donor fluorescence emission ($1/\tau_d$) and τ_d is the lifetime of the donor.

Energy transfer efficiency (*E*) is a function of R_o (Eqn 14); it is monitored via a change in donor intensity (Eqn 15), or lifetime (Eqn 16).

$$E = \left[\frac{R_o^6}{R_o^6 + r^6}\right] \tag{14}$$

$$E = 1 - (I_{da}/I_d) \tag{15}$$

$$E = 1 - (\tau_{da} / \tau_{d}) \quad (16)$$

where I_{da} is the intensity of the donor in the presence of acceptor, τ_{da} is the lifetime of the donor in the presence of the acceptor, I_a is the intensity of the acceptor in the absence of donor (at the donor excitation wavelength), I_{da} is the intensity of the acceptor in the presence of the donor and ϵ_d is the exctinction coefficient of the donor.

The energy transfer efficiency (E) has a sixth power dependence in R_o, which means that E falls off very rapidly beyond R_o (Fig. 3a; Eqn 14). Consequently, organic dye energy transfer pairs (e.g. fluorescein–TMR, R_o = 55 Å) are limited to systems in which donor and acceptor are close

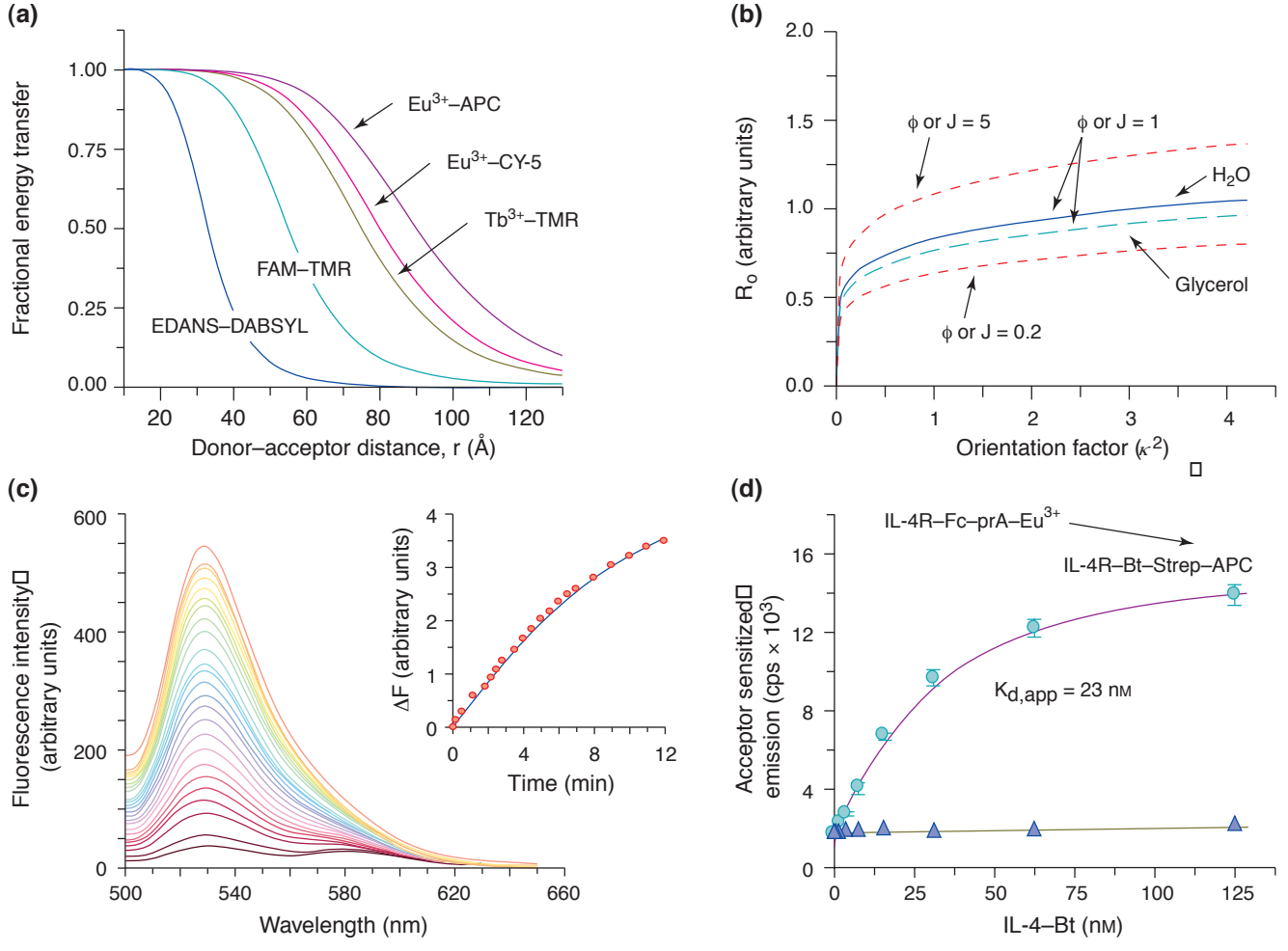

Figure 3. *Simulated and real examples of resonance energy transfer. (a) Predicted relationship between donor–acceptor distance and energy transfer for a range of commonly used donor–acceptor pairs. (b) Predicted sensitivity of distance for half energy transfer (R_o) on the donor–acceptor orientation (κ^2), spectral overlap (J, arbitrary units), quantum yield of donor (Φ_d), and refractive index (n; shown in the range 0–100% glycerol). (c) Primary data from a protease assay based on the short-range energy transfer pair fluorescein–TMR peptide substrate (donor and acceptor are separated in the linear extended peptide by ~46 Å). The data show relief of donor quenching (~20-fold) during a protease cleavage time course. (d) Long-range energy transfer assay for binding of biotinylated interleukin 4 (IL-4-Bt) to an IL-4 receptor–Fc (IL-4R–Fc) fusion protein, where the donor (Eu^{3+}-chelate) and acceptor (allophycocyanin, APC) are indirectly supplied via protein-A (prA) and streptavidin, respectively. The figure shows titration of IL-4-Bt at fixed IL-4R–Fc–prA-Eu^{3+}, yielding a $K_{d,app}$ of 23 nM. Error bars show SD.*

and with fairly defined separation, such as in peptide substrates for proteases. An example of primary data from such a system is given in Fig. 3c, which shows cleavage of a 12-mer peptide protease substrate labelled on either side of the protease cleavage site with fluorescein and TMR, respectively.

The longer R_o provided by Ln^{3+}-based time-resolved energy transfer systems (TRET; Fig. 3a) means that protein–protein interactions using indirect labelling (and generally less specific placement of donor–acceptor) can be used successfully. Figure 3d shows an example of such a system in which binding of biotinylated (Bt) interleukin 4 (IL-4) to an IL-4 receptor (IL-4R)–Fc fusion was measured and where the donor (a Eu^{3+}-chelate) and acceptor (APC) were supplied as conjugates with protein-A and streptavidin, respectively.

A major additional advantage of TRET systems arises from separation of donor–acceptor lifetime from background signals (e.g. autofluorescent compounds, instrument artefacts, plastics, etc.) and from the effective amplification of acceptor emission when $\tau_d \gg \tau_a$, particularly when the acceptor is a highly efficient fluor (Eqns 15,16; e.g. APC: $\epsilon_{650} = 7 \times 10^5\ M^{-1}\ cm^{-1}$). In binding assays this means that, at least in principle, amplification of the sensitized emission signal from the ligand–receptor binary complex (being much brighter than the donor) can allow signals to be detected at low fractional binding (e.g. if the K_d is high). This contrasts with other homogeneous techniques that typically lack signal amplification between free and bound species (e.g. FP, FCS) and which therefore require significant fractional binding for robust assays.

Fluorescence anisotropy (polarization) basics

Fluorescence polarization (FP) and anisotropy (FA) are merely different names (and units) for the same process. When a fluorophore is excited with polarized light, the emitted light is also polarized. This is because fluorophores are specifically excited according to their molecular orientation relative to the direction of the polarization of the excitation light. Rotational diffusion of a fluorophore (or fluorescence-labelled analyte) leads to depolarization of fluorescence. Fluorescence polarization-based assays have become used for HTS subsequent to the recent availability of MTP readers. Polarization (anisotropy) is a function of molecular properties, most specifically Brownian molecular rotation (see above). Some of the relevant formalisms follow.

Polarization (P) and anisotropy (r) are interchangeable

$$P = (I_\parallel - I_\perp)/(I_\parallel + I_\perp) \quad (17)$$

$$r = (I_\parallel - I_\perp)/(I_\parallel + 2I_\perp) \quad (18)$$

where $I_\parallel$ and $I_\perp$ are the emission intensity parallel and perpendicular, respectively, to the plane of excitation light.

Therefore

$$P = 3r/(2 + r) \quad (19)$$

$$r = 2P/(3 - P) \quad (20)$$

Anisotropy is a preferable unit for all quantitative measurements because the equations that describe it are considerably simpler; for example, compare these Perrin equations for polarization and anisotropy.

$$1/P - 1/3 = (1/P_0 - 1/3)(1 + \tau_F/\tau_c) \quad (21)$$

$$r_0/r = 1 + \tau_F/\tau_c \quad (22)$$

where P_0 is the initial limiting polarization of the fluorophore (normally ~0.35), ρ is the rotational relaxation time, r_0 is the limiting anisotropy (normally ~0.25), and τ_c is rotational correlation time.

This becomes very important in binding reactions when the concentration of two components (e.g. bound and free) must be determined quantitatively (see following section on binding reactions). Limiting anisotropy (or polarization) varies with wavelength, dye and instrument and is typically ~0.25 for fluorescein/TMR.

Anisotropy is a function of the molecular rotational relaxation time (ρ) or rotational correlation time (τ_c) relative to the fluorophore lifetime, τ_F (e.g. Fig. 4a, Eqns 21,22). As ρ is directly related to mass (again assuming spherical geometry; see section on macromolecular properties), anisotropy values can be predicted and are almost linearly related to protein mass until ρ approaches τ_F. Rotational relaxation time should not be confused with the related term rotational correlation time ($\tau_c = \rho/3$). Both are often used in the literature. In addition, τ_F should not be confused with the terms used to describe FCS correlation times (e.g. τ_i; see next section).

Fluorophore lifetime is the key factor in determining anisotropy values (Fig. 4a,b). Short lifetime dyes (e.g. fluorescein/rhodamine: τ_F ~4 ns) rapidly approach a limiting value at a globular protein mass of ~50 kDa (Fig. 5b) and are thus unsuitable for most protein–protein

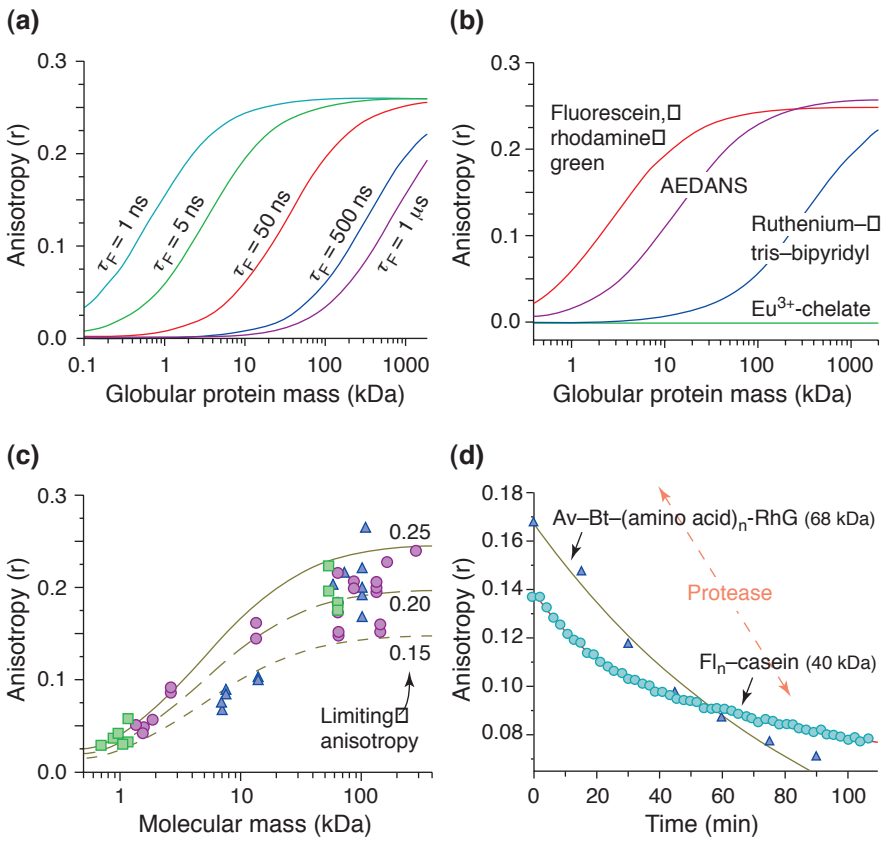

Figure 4. *Simulated and real examples of fluorescence anisotropy measurements. (a) Calculated effect of fluorescence lifetime (τ_F) on anisotropy as a function of globular protein mass. (b) Similar calculations for commonly used fluorophores (assuming the following values for τ_F: fluorescein/rhodamine, 4 ns; AEDANS, 20 ns; ruthenium–tris–bipyridyl, 500 ns; Eu^{3+}-chelate, 1000 μs). (c) Survey of observed anisotropy values from a selection of fluorescein/rhodamine green-based assays developed at SmithKline Beecham; triangles show a nucleic acid, squares show a low molecular weight ligand or complex and circles show a protein or peptide. Lines show the predicted relationship between globular protein mass and anisotropy [i.e. from (b)], assuming τ_F = 4 ns and limiting anisotropy values as shown. (d) Time course from two types of protease assay monitored using anisotropy. Av, avidin; Bt, biotin; Fl, fluorescein; RhG, rhodamine green.*

Predictions of anisotropy are generally reasonably reliable. Figure 4c shows a survey of anisotropy values plotted against mass for a range of fluorophore-labelled ligands and their complexes taken from more than 20 anisotropy assays that we have configured. These data are fairly well described by the predicted anisotropy, particularly if slightly lower values are assumed for the limiting anisotropy. However, the formalisms in every case underestimate measured anisotropy to some extent. This has several origins. First, local motion of the fluorophore (so called 'propeller effects') can reduce the observed polarization/anisotropy. Second, many of the reagents shown in Fig. 4c have highly asymmetric shapes (e.g. oligonucleotides), in which the value of ρ will be seriously underestimated because of axial as well as end-to-end Brownian rotation. In addition, self-quenching in multi-labelled molecules (e.g. proteins labelled with a stoichiometry >1 via conventional amine reactive reagents) leads to depolarization.

Binding reactions monitored by anisotropy

Anisotropy measurements are typically used in assays either to monitor hydrolytic reactions (e.g. the protease assays shown in Fig. 4d) or for binding reactions.

In designing anisotropy-based binding assays, several factors must be taken into account, including the mass change induced upon binding, the absolute mass of the components, the concentration of fluorophore required for robust detection (in the presence of test compounds), and the K_d of the interaction.

Historically polarization has been used, but anisotropy is preferable for all quantitative measurements in two- (or more) component systems because the observed anisotropy (A_{obs}) is the simple sum of anisotropies of individual components, weighted by their brightness (Eqn 23). For polarization [(P_{obs}); Eqn 24] the relationship is not so

or indirect-labelling applications. Very long lifetime fluors (e.g. ruthenium or lanthanide complexes) have the opposite problem, in that it is difficult to achieve anisotropy changes without complexation to a very large system (e.g. membrane particle, cell or bead) or immobilization (see Fig. 5b). Intermediate lifetime dyes such as AEDANS (Fig. 5b) tend not to have useful wavelengths for screening applications, but have been widely used in fundamental characterization of protein–protein interactions[10].

simple, as such distortions can result if the components differ in brightness (e.g. one is quenched upon binding) – as commonly happens.

$$A_{obs} = \sum F_I A_I \tag{23}$$

$$\left(\frac{1}{P_{obs}} - \frac{1}{3}\right)^{-1} = \sum_i \frac{F_i}{(1/P_i) - (1/3)} \tag{24}$$

where F_i is the fractional contribution of species i to the total intensity, and A_i and P_i are the intrinsic anisotropy and polarization of species i.

Even when using anisotropy, any changes in brightness between free and bound fluorophore–ligand forms need to be measured and taken carefully into account when measuring binding and displacement isotherms (Eqns 25–31), for example, in the scheme:

$$E + L \underset{}{\overset{K_L}{\rightleftharpoons}} EL$$

$$A_{obs} = \{A_1([L_t]–[EL]) + A_2\, Q[EL]\}/([L_t]–[EL] + Q[EL]) \tag{25}$$

and

$$[EL] = ((K_L + [L_t] + [E_t]) – \{(K_L + [L_t] + [E_t])^2 – 4[L_t][E_t]\})/2 \tag{26}$$

where $B = K_L + [L_t] + [E_t]$

and where A_1 and A_2 are the respective anisotropies of L and EL, $[L_t]$ is the total fluorophore concentration and Q is the ratio of their respective quantum yields (i.e. Φ_{EL}/Φ_E).

Thus at 0, 50 and 100% binding we obtain:

$$A_{obs,o} = A_1\,[L_t]/[L_t] \tag{27}$$

$$A_{obs,50} = (A_1 + A_2 Q)/(1 + Q) \tag{28}$$

$$A_{obs,100} = A_2 Q[EL]/Q[EL] \tag{29}$$

For displacement by a competitive ligand X with binding constant, K_x, total concentration $[X_t]$ and free concentration [X], the mass conversation expressions become $[E] = [E_t] – [EL] – [EX]$ and $[X] = [X_t] – [EX]$. Eqns 30 and 31 now define [EL] and [EX], whereby substitution of Eqn 31 into Eqn 30 allows the observed anisotropy to be subsequently calculated from Eqn 25:

$$[EL] = ((K_L + [L_t] + [E_t]–[EX]) – \sqrt{((K_L + [L_t] + [E_t]–[EX])^2 – 4[L_t]([E_t]–[EX])})/2 \tag{30}$$

where $C = K_L + [L_t] + [E_t] – [EX]$

$$[EX] = ((K_x + [X_t] + [E_t]–[EL]) – \sqrt{((K_x + [X_t] + [E_t]–[EL])^2 – 4[X_t]([E_t]–[EL])})/2 \tag{31}$$

where $D = K_X + [X_t] + [E_t] – [EL]$

These equations, and the simulations given in Fig. 5a, show that when intensity bound/intensity free (Q) is not equal to 1, the apparent K_d ($K_{d,app}$) determined in binding curves without brightness correction is not equal to the true K_d. This results in an offset of $K_{d,app} = K_d(1/Q)$, and hence errors in the estimation of K_d. If uncorrected, this would be problematic in cases where K_d is overestimated (i.e. when the fluoroligand is quenched upon binding). In such a case, binding assays would probably be established at [receptor, R_t] $> K_d$ to yield a measurable anisotropy change and as a result would be less sensitive to competitive ligands, because in the limit of $[R_t] \gg$[fluorescent ligand], the $K_{i,app}$ for a competitive inhibitor would be: $K_{i,app} \sim K_i(1+[R_t]/K_d)$. Similar considerations apply under all conditions of receptor, ligand, inhibitor and K_d values described quantitatively by Eqns 25, 30 and 31.

Figure 5c,d show a typical example of the types of distortion that can occur if the value of Q is far from unity and not corrected for. In this case, Q was ~0.2 and so binding could actually be measured readily using FLINT (Fig. 5e). Both FLINT and corrected anisotropy yield a K_d of ~100 nM. The observed $K_{d,app}$ from uncorrected polarization (~500 nM; Fig. 5d) was therefore as expected from Q ~0.2.

As the anisotropy is a weighted average of two values (intrinsic anisotropy of bound and free) with typically comparable (<4-fold) magnitude, there is a requirement to induce considerable fractional binding to generate a useful signal change. In our experience, this is a Δr of ~0.08 for robust HTS which, if screening at the K_d, means that a maximum signal change of ~0.16 is required. Given that the working range of most MTP-based FP readers in an HTS environment (i.e. in the presence of test compounds) is ~1–100 nM fluorophore, constraints are imposed upon the range of K_ds that are accessible. In addition, to achieve the desired signal range (with an effective limiting anisotropy of ~0.2–0.25), the ligand must clearly be relatively small when using a short lifetime fluorophore such as fluorescein or rhodamine. Figure 5b shows examples of two

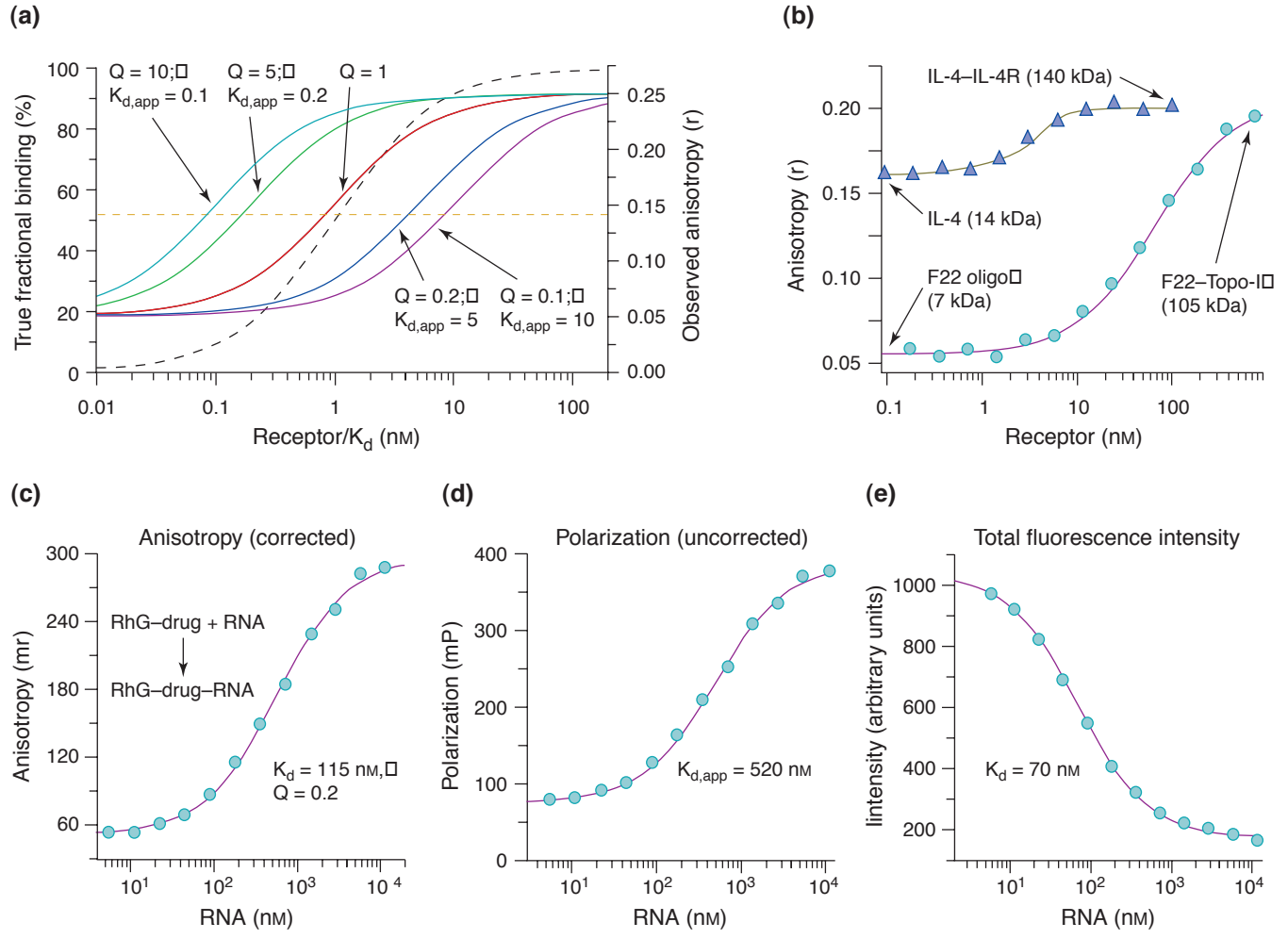

Figure 5. *Simulated and real examples of anisotropy-based binding assays. (a) Distortions in anisotropy binding curves caused by (uncorrected) changes in intensity of bound and free species ($Q = I_{bound}/I_{free}$). The true fractional binding (dotted curve) and the simulated anisotropy isotherms as a function of Q with $R_{free} = 0.05$ and $R_{bound} = 0.25$ (solid curves) are shown. (b) Two examples of binding isotherms where the available signal amplitude is limited by the anisotropy of the fluoroligand. (c–e) Example of distortion in anisotropy/polarization experiments when changes in Φ_F upon binding are not corrected. In this case, Q ~0.2. (c) Corrected anisotropy binding isotherm, yielding K_d = 115 nM. (d) Uncorrected polarization isotherm, resulting in a ~5-fold overestimate of K_d. (e) Total intensity during titration of receptor into ligand, showing the extent of quenching upon binding and yielding a K_d of ~70 nM.*

anisotropy binding assays in which the total amplitude of Δr is determined largely by the anisotropy of the fluoroligand (which in one case is already relatively highly polarized). Even when using a small ligand, local motion effects can make the anisotropy of the ligand–receptor complex lower than expected. A useful technique to overcome this is to introduce additional components (e.g. an antibody directed towards an expressed epitope tag on the receptor) that increases the mass of the binary complex and therefore the Δr amplitude. One way in which the flexibility of anisotropy binding assays might be extended in the future is by the use of longer lifetime fluors (e.g. ruthenium complexes; see Fig. 4b).

Fluorescence correlation spectroscopy

In FCS measurements, temporal fluctuations in the fluorescence signal detected from the diffusion of individual fluorescent molecules into and out of a small tightly focused confocal element (detection volume typically ~1 fl) are analysed using autocorrelation techniques[7,8]. In

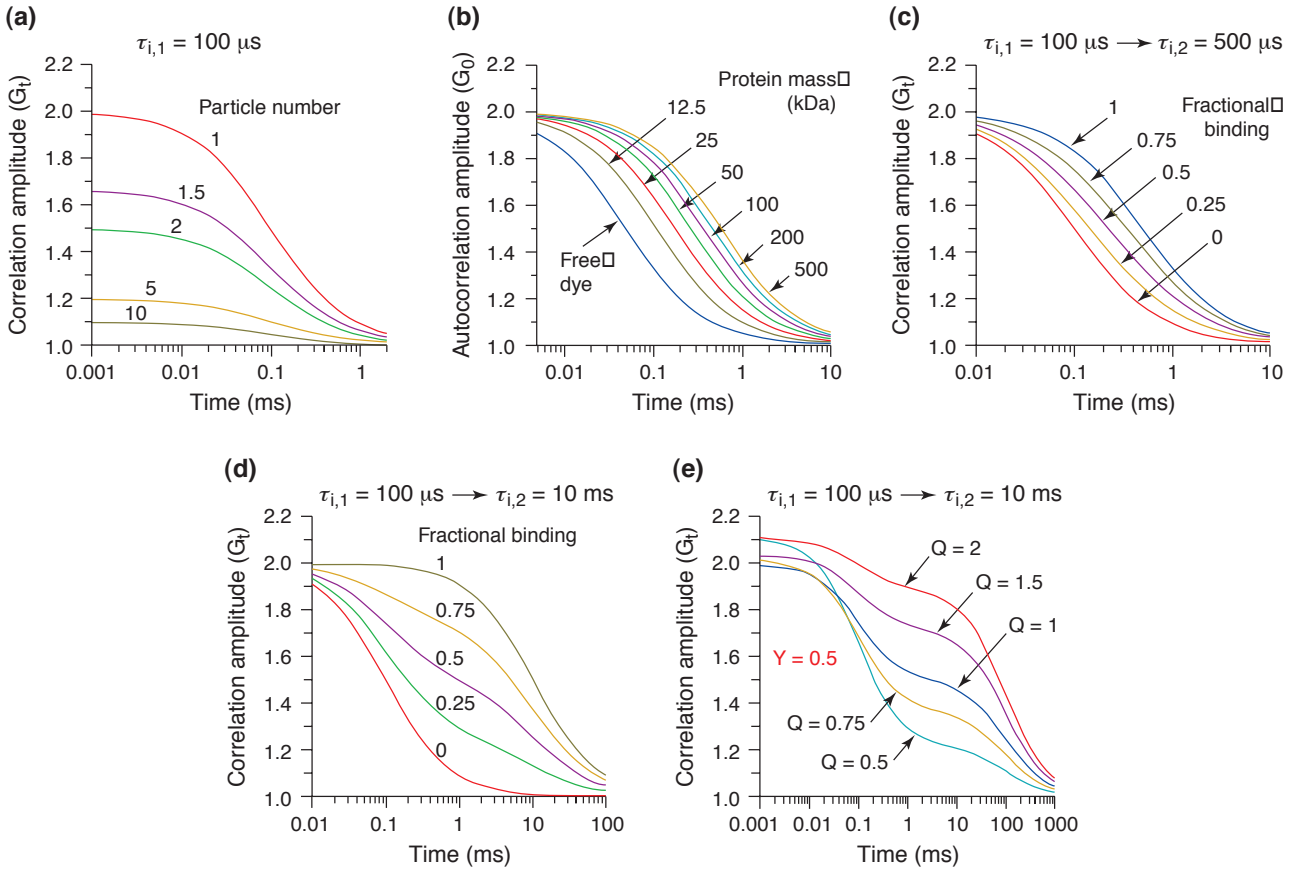

Figure 6. *Simulated results from fluorescence correlation spectroscopy (FCS). (a) Effect of particle number (i.e. fluorophore concentration, here in the range ~1–10 nM) on the amplitude of FCS correlation curves. (b) FCS correlation curves for globular proteins, showing the change in* τ_i *as a function of mass (M). (c) Two-component FCS curves for a typical binding reaction (e.g.* $\tau_{i,1}$ *= 100 μs; M ~10 kDa >* $\tau_{i,2}$ *= 500 μs; M ~200 kDa. (d) Simulated two-component FCS curves as in (c), but with* $\tau_{i,2}$ *= 10 ms. Note that this value is far greater than would normally be measured in real experiments, and is shown for illustrative purposes only. (e) Effect of changes in brightness two components in FCS fits (Q =* cpm_2/cpm_1*; i.e. brightness bound/brightness free) where Y (fractional binding) = 0.5 and using the same values of* $\tau_{i,1}$ *and* $\tau_{i,2}$ *as in (d).*

principle, this provides a uniquely information-rich output. The FCS autocorrelation function yields information including the concentration (N, average number of fluorophore molecules in the detection element), the diffusion time of components (e.g. $\tau_{i,1}$, $\tau_{i,2}$) and the average brightness per molecule (cpm). Below we comment on each of these parameters and summarize the most relevant formalisms. Figures 6 and 7 show examples of simulated and real FCS assay data.

The correlation amplitude for a single fluorophore in three dimensions (G_t) is given as:

$$G_t = 1 + \frac{1}{N} \cdot \frac{1}{1 + 4Dt/\omega_r^2} \left(\frac{1}{1 + 4Dt/\omega_l^2} \right)^{1/2} \quad (32)$$

The simplified two-dimensional form is:

$$G_t = 1 + \frac{1}{N} \left(\frac{1}{1 + (t/\tau_i)} \right) \quad (33)$$

And the fluorophore concentration (C) is:

$$C = N/N_a V \quad (34)$$

The correlation amplitude for a mixture of components in two dimensions (G_0) is[6–8]:

$$G_t = 1 + \frac{1}{N} \left(\frac{1-Y}{1 + (t/\tau_{i,1})} \cdot \frac{Y}{1 + (t/\tau_{i,2})} \right) \quad (35)$$

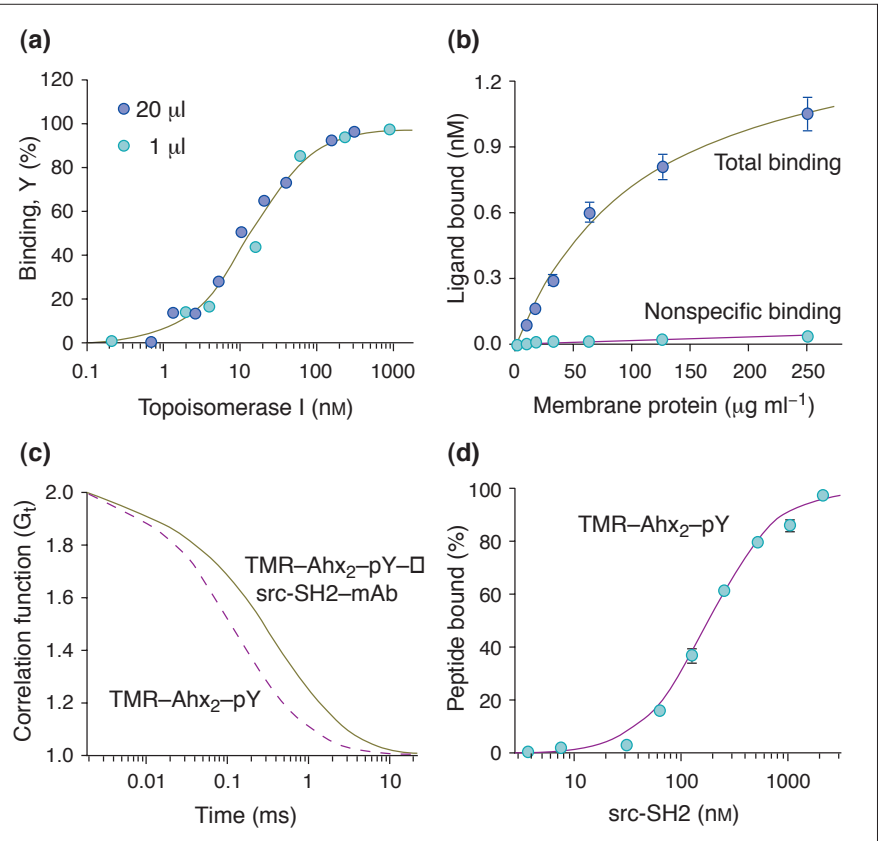

Figure 7. *Actual results from fluorescence correlation spectroscopy (FCS) assays. (a) Binding of fluor-oligonucleotide to topoisomerase-I, conducted in a total assay volume of either 1 or 20 µl. (b) TMR–7-transmembrane ligand binding to its receptor (on membrane vesicles). (c) Correlation curves of free and bound fluorescently labelled phosphopeptide, TMR–Ahx$_2$–pY and (d) its binding isotherm to src-SH2–mAb complex. Error bars show* SD.

where N is the number of fluorescent molecules in the detected element of volume (V), D is the diffusion coefficient ($= \omega_r^2/4\tau_i$), ω_r is the radius of the confocal volume element in the xy dimension, ω_l is the radius (or half-length) in the z dimension, t is the time channel, N_a is Avagadro's number (6.022×10^{23} mol^{-1}), τ_i is fluorophore correlation time ($\tau_{i,1}$, $\tau_{i,2}$ etc. for individual species: e.g. free, bound), and Y is fractional concentration of components (e.g. [bound]/[free] + [bound]).

The autocorrelation amplitude (G_0) yielded in FCS experiments is inversely related to fluorophore concentration (Eqns 32,33,35), as illustrated by the simulation shown in Fig. 6a. This is intuitive: as the average particle number (N) increases, the extent of signal *fluctuations* with time gradually disappears. Therefore the sensitivity of FCS actually increases with decreasing fluor concentration, which is unique to this technique. Conversely, this limits the upper concentration of fluor that can be used (dependent upon confocal volume; typically 0.1 µM). At very low fluor concentrations (e.g. <0.5 nM fluorescein/rhodamine), FCS assays become limited by the reading time required for sufficient molecular encounters to accurately define the autocorrelation function (fluor at 0.1 nM in a volume of 1 fl, N ~0.1). Both the upper and (practical) lower limits on fluor concentration are to some extent a function of the confocal volume size (within the limits of the optics) and so can be adjusted to extend these boundaries. FCS is unique in providing an absolute solution to the number of fluorescent particles and therefore concentrations of assay components that can be used for quality control processes.

A major advantage for FCS in miniaturized uHTS is that the signal output (arising from ~1 fl) is completely insensitive to miniaturization to and beyond the lower limits of discrete well-based HTS (probably ~1 µl, limited by liquid handling, evaporation, etc.). Figure 7a shows an example of identical performance for a binding assay performed in volumes of 1 and 20 µl.

The observed diffusion time (τ_i) is a function of the diffusion coefficient (D) of the observed molecular species and the size of the confocal volume element. Taking again the simplifying assumption of globular proteins, τ_i is directly related to molecular radius (r) and hence the cubed root of M (see section on macromolecular properties; Fig. 2b). FCS is therefore somewhat less sensitive to ΔM than fluorescence anisotropy, the latter being almost directly related to M (within its useful range; see previous section). However, in FCS experiments, the restrictions in signal generation encountered as the limiting values are approached in anisotropy do not occur, so much larger particles (e.g. beads, membrane vesicles; see also Fig. 6) can be analyzed. In the absence of an oscillating beam set-up, the major limitation becomes the time to encounter sufficient fluorophore bursts at any given concentration, because the number of encounters per unit time is related to D and therefore decreases sharply with M (e.g. Fig. 2b). Figure 6b shows simulated correlation curves for proteins of different size. The dependence of τ_i in M can make the

individual components in FCS fits difficult to discern by eye (e.g. Fig. 6c). However, provided $\Delta M > 10$-fold, both components can normally be robustly defined. Figure 6d shows a simulated binding experiment in which the bound diffusion time, $\tau_{I,i}$, has been made artificially large for illustrative purposes. Examples of actual FCS binding data are shown in Fig. 7.

For two-component systems (e.g. binding of fluoroligand to receptor), FCS data yield explicitly the concentrations of both components (Eqn 35). However, as with fluorescence anisotropy, a change in quantum yield upon binding (recall the term Q = intensity bound/intensity free; see above) will result in distortions unless corrected using similar approaches to those already described. However, in this case, the mathematical relationships are different: the contribution to signal amplitude from each fluorophore species is proportional to concentration and the square of 'detectivity' (e.g. brightness; Eqn 36).

$$G_0 = \frac{\sum \mathrm{cpm}_i^2 N_i}{\left(\sum \mathrm{cpm}_i N_i\right)^2} \qquad (36)$$

where G_0 is full-scale amplitude at t = 0, cpm_i is the detectivity (i.e. brightness) of fluorophore i, N_i is number of molecules of fluorophore i in the volume element.

FCS measurements of particles of different brightness are therefore strongly weighted in favour of the brighter component (more so than anisotropy). Figure 6e shows an example of this. In binding reactions where the value of Q deviates markedly from unity, it is therefore necessary to employ a correction (e.g. Eqn 37).

$$G_t = 1 + \frac{1}{N[(1-Y)+YQ]^2}\left(\frac{1-Y}{1+(t/\tau_{i,1})} \cdot \frac{YQ^2}{1+(t/\tau_{i,2})}\right) \qquad (37)$$

where terms are as described for Eqns 32–35.

Conversely, for uHTS applications in the presence of test compounds, the effective weighting against dim particles (e.g. autofluorescent test compounds) has a benefit in that these are underrepresented. One additional benefit for compound testing is that the effective pathlength of the confocal volume element is ~200 μm and so inner-filter effects on intensity are seldom observed.

One restriction on the analysis of quantal bursts in FCS is that the lifetime (τ_F) of the fluorophore must be less than its diffusion time through the confocal volume (τ_a). In practice, this means that only prompt fluors ($\tau_F \ll 10$ ns) are used.

In addition to information on concentration and diffusion times, FCS autocorrelation curves also yield average molecular brightness. In systems in which $Q \neq 1$, changes in brightness can themselves be used to configure assays. Evotec BioSystems (Hamburg, Germany)[13] has recently developed a more advanced analysis of the discrete molecular brightness components. This is an exciting advance because it opens the way to mass-independent FCS assays. In addition, other FCS-based techniques such as fluctuation anisotropy, and con-focal fluorescence coincidence analysis (CFCA)[14] and two-colour cross-correlation[15] look certain to further extend the cope of this technique for uHTS in the future.

Conclusions

This review has described, at least in outline, some of the most important formalisms that describe signal origins in fluorescence techniques being widely adopted as the major future readout strategy for HTS. Although, the foregoing contains several assumptions and oversimplifications, the real examples of assay data shown illustrate the value of approaching assay design in this way.

ACKNOWLEDGEMENTS

We thank Steve Ashman, Sandra Turconi, Martin Ruediger, Jonathan Saunders and Farid Khan for providing the data shown herein.

REFERENCES

1 Mathis, G. (1995) *Clin. Chem.* 41, 1391
2 Mellor, G.W. *et al.* (1998) *J. Biomol. Screening* 3, 91–99
3 Hemilla, I. and Webb, S. (1997) *Drug Discovery Today* 2, 373–381
4 Lacowicz, J.R. (1983) *Principles of Fluorescence Spectroscopy*, Plenum Press
5 Holzwarth, A.R. (1995) *Methods Enzymol.* 246, 334–362
6 Auer, M. *et al.* (1998) *Drug Discovery Today* 3, 457–465
7 Eigen, M. and Rigler, R. (1994) *Proc. Natl. Acad. Sci. U. S. A.* 91, 5740–5747
8 Maiti, S., Haupts, U. and Webb, W.W. (1997) *Proc. Natl. Acad. Sci. U. S. A.* 94, 11753–11757
9 Beecham, J.M., Knutson, J.R. and Brand, L. (1986) *Biochem. Soc. Trans.* 14, 832–835
10 Selvin, P.R. (1995) *Methods Enzymol.* 246, 300–334
11 Stryer, L. (1978) *Annu. Rev. Biochem.* 47, 819
12 Förster, T. (1948) *Ann. Phys.* 2, 55–75
13 Evotec (1996) *International Patent WO 98/16814*
14 Winkler, T. *et al.* (1999) *Proc. Natl. Acad. Sci. U. S. A.* 96, 1375–1378
15 Kettling, U. *et al.* (1998) *Proc. Natl. Acad. Sci. U. S. A.* 95, 1416–1420